

Title: Global record of ‘ghost’ nanofossils reveals plankton resilience to high- CO₂ and warming

Authors: Sam M. Slater^{1*}, Paul Bown², Richard J. Twitchett³, Silvia Danise⁴ & Vivi Vajda¹

5 **Affiliations:**

¹Department of Palaeobiology, Swedish Museum of Natural History; Stockholm, SE-104 05, Sweden.

²Department of Earth Sciences, University College London; London, WC1E 6BT, UK.

³Department of Earth Sciences, The Natural History Museum; London, SW7 5BD, UK.

10 ⁴Dipartimento di Scienze della Terra, Università degli Studi di Firenze; Via La Pira 4 50121, Firenze, Italy.

*Corresponding author. Email: sam.slater@nrm.se.

Abstract: Predictions of how marine calcifying organisms will respond to climate change rely
15 heavily on the fossil record of nannoplankton. Declines in nanofossil abundance and calcium carbonate (CaCO₃) through several past global warming events have been interpreted as ‘biocalcification crises’ caused by ocean acidification and related factors. We present a global record of imprint, or ‘ghost’, nanofossils that oppose this view, revealing exquisitely preserved nannoplankton throughout an inferred Jurassic biocalcification crisis. Imprints from two further
20 Cretaceous warming events confirm that the fossil records of these intervals have been strongly distorted by CaCO₃ dissolution. Although the rapidity of current climate change exceeds the

temporal resolution of most fossil records, making direct comparison with past warming events challenging, our findings demonstrate that nannoplankton were more resilient to past events than traditional fossil evidence would suggest.

- 5 **One-Sentence Summary:** Discovery of plankton imprint fossils challenges inferred links between past global warming events and biocalcification crises.

Main Text: As CO₂-levels in the atmosphere rise, resultant ocean acidification (OA) and declining seawater carbonate ion concentrations will likely make it more difficult for marine organisms to form their calcium carbonate (CaCO₃) skeletons or shells (1, 2). Coccolithophores, a group of unicellular phytoplanktonic algae (also known as nanoplankton), are the most productive marine calcifiers (3), but predicting their response to future environmental change has proved challenging. Experiments testing the effects of high-CO₂ and temperatures on living coccolithophores and their calcitic exoskeletons have shown apparently contradictory results within and between species (4–8). However, interpretations of geological and fossil-based evidence have evoked globally catastrophic responses in nanoplankton during past intervals of high temperature and CO₂ (reviewed in Data S1 to S3). Specifically, prominent studies have observed major declines in CaCO₃ and nanoplankton abundance through past global warming events, and interpreted these signals as ‘biocalcification crises’, whereby OA, and related environmental change, directly compromised biogenic CaCO₃ production. Contrary to this, others have argued that these declines in CaCO₃ are caused by dissolution of carbonate at the seafloor during these events, and that independent evidence for nanoplankton responses to OA needs to be better understood and demonstrated before biocalcification crises are invoked (9, 10). However, the biocalcification crisis paradigm continues to be widely applied to past warming episodes, especially the Mesozoic oceanic anoxic events (OAEs; Data S1 to S3), and given that this model predicts potentially disastrous changes to future marine biodiversity and carbon cycle function, we tested this hypothesis using a novel methodology.

We examined one of the most severe reported biocalcification crises of the last 200 million years, associated with the Toarcian Oceanic Anoxic Event (T-OAE; ~183 million years ago [Ma]) in the Early Jurassic. The T-OAE was a geologically-rapid global warming event caused by volcanism in the Southern Hemisphere (11), and is characterized by a range of environmental,

geological and ecological changes, including high-CO₂, OA, oceanic anoxia, the deposition of organic-rich sediments, a major negative carbon isotope excursion, and widespread extinction (12 and references therein). Previous interpretations of the biocalcification crisis are primarily based on declining CaCO₃ in the sedimentary rock record and decreased nanoplankton species abundances and sizes (Data S1), but crucially this evidence has relied upon conventional nanofossil analyses, whereby data are derived from calcite ‘body’ fossils. Here we report on an overlooked form of preservation, namely imprint, or ‘ghost’ nanofossils, which provides critical information that may be lost from the more routinely studied ‘body’ fossil record.

Toarcian rock samples from the UK, Germany, Japan and New Zealand (Fig. S1) were processed for organic matter analysis. Scanning electron microscopy (SEM) of organic particles revealed nanoplankton imprints preserved on the surfaces of marine organic-walled plankton (dinoflagellate cysts, prasinophytes and acritarchs), amorphous organic matter (AOM), and spores and pollen from land plants (Fig. 1). Imprints are also visible using transmitted-light, fluorescence, and confocal microscopy (Fig. S2), but exquisite details are evident using SEM, with specimens displaying diagnostic coccolith rims, radial and imbricating sutures, and fragile axial and radiating central structures (Figs. S3 to S12). Preservation is often pristine, and digital inversion of imprint images provides ‘virtual casts’ that assist in visualization and identification of the original nanofossils (Fig. 1). Imprints were found as single or multiple specimens of the same or different species and cover a range of forms, including small coccoliths (< 3 μm, Fig. S3I), larger nanoplankton (Figs. S3J-O and S8A-D) and collapsed coccolithophore exoskeletons (coccospheres) (Figs. S5A-B and S8F). Nanoplankton imprints on organic matter have only occasionally been reported from the fossil record (13–15), presumably because of their cryptic mode of preservation and minute size. Some studies have interpreted imprints as the negative molds of coccoliths that were dissolved during acid digestion of rock samples in the laboratory

(14). However, we record imprints on unprocessed rock surfaces (Fig. S6) and in samples devoid of CaCO_3 , showing these fossils occur naturally.

Reduced nanoplankton abundances during the T-OAE have been reported from multiple locations (Data S1), but this signal is most extreme in the Cleveland Basin, Yorkshire (UK), where a nanoplankton ‘disappearance event’ has been observed (16). Samples from Yorkshire, studied here using traditional nanoplankton ‘body’ fossil methods, were either barren, or yielded ‘rare’ or ‘very rare’ nanofossils (Figs. S13 and S14). These observations essentially replicate previous findings of reduced species abundances or absences throughout the T-OAE (17), and seemingly support the biocalcification crisis paradigm. However, imprints from the same samples challenge this view, revealing abundant and rich nanoplankton communities throughout the T-OAE interval, refuting the ‘disappearance event’ hypothesis. Imprints are not just confined to the Cleveland Basin but have been discovered in a wide range of depositional settings in globally-distributed T-OAE strata (e.g. Germany, Japan and New Zealand, Figs. 1 and 2). These results indicate that observed decreases in CaCO_3 and nanofossil abundance through the T-OAE are due to CaCO_3 dissolution after burial, rather than representing a primary crisis of the living nanoplankton. The imprint fossils from Japan and New Zealand (Fig. 1) are the oldest coccoliths recorded from these countries, demonstrating that this approach is widely applicable and can expand nanofossil records, even in rocks where ‘body’ fossils are absent and have been subjected to thermal alteration (e.g. Japanese material studied here [17]).

We further extended our study to test for imprints through two Cretaceous OAEs, the early Aptian OAE1a (~120 Ma) and the Cenomanian-Turonian OAE2 (~94 Ma), for which there are also claims for biocalcification crises (reviewed in Data S2 and S3). The Cretaceous OAEs are also associated with distinct episodes of volcanism, and characterized by comparable suites of environmental, geological and ecological changes (12 and references therein). We found imprint

fossils through both Cretaceous OAEs (Figs. 1 and 2, Figs. S11 and S12), demonstrating that ‘ghost’ nanofossil preservation is not limited to the T-OAE, and that observed decreases in CaCO₃ and nanoplankton abundances during OAE1a and OAE2 (Data S1 to S3) are likely also linked to the secondary removal of CaCO₃ from the rock record. Imprints from OAE2 of Contessa, Italy, are particularly important because these were recorded during an inferred nanoplankton biocalcification ‘blackout’, corresponding to the Bonarelli Level, a ~1-meter-thick black shale virtually devoid of CaCO₃, which abruptly interrupts a limestone succession rich in ‘body’ fossils (Fig. S14, Data S3). Our results overturn the blackout hypothesis and indicate that the original CaCO₃ has been lost through post-burial dissolution, leaving a misleading signal of declining carbonate production during OAE2.

The recurrence of imprints in OAE-related sediments demonstrates that these organic-rich intervals are especially prone to this type of nanofossil preservation, indeed the OAE intervals record the richest imprint assemblages. Abundances of imprints and AOM generally positively correlate (Fig. S15), suggesting that plentiful organic matter was an important requirement, providing the necessary ‘plastic’ substrate for imprinting. This also explains the subsequent dissolution of CaCO₃, as high organic matter content can lead to acidic pore waters during diagenesis (18). The formation of imprints also required overburden pressure prior to the loss of the ‘body’ fossils, indicating that dissolution took place after burial, and the absence of compressed imprints reveals that this occurred after lithification.

Nanofossil abundances in sedimentary rocks are the product of a range of factors, including those that affect original populations (temperature, nutrients, water chemistry), export pathways (grazing, ballasting), secondary abundances (exported plankton *versus* siliciclastic dilution) and preservation (diagenesis). None of these factors necessarily disrupts calcification in the living nanoplankton and therefore preserved abundance changes alone do not provide

evidence of biocalcification crises. On the contrary, our observations show that CaCO₃ and nanoplankton ‘body’ fossil abundances can be severely modified or eradicated following deposition, indicating that these records are unreliable proxies for OA or pelagic carbonate production. Independent geochemical proxy evidence for OA at the T-OAE remains contentious (19, 20), and given the uncertainty over rates of carbon injection that drove this and other OAEs, these rates may well have been too slow to have induced prolonged or high magnitude surface water OA (10, 21). However, regardless of the severity or duration of OA during the T-OAE, or indeed other proposed causes of a nanoplankton crisis, such as changes in temperature, salinity, nutrients or anoxia (see Data S1), our records challenge the concept of a crisis. More generally, these findings call for the re-examination of other inferred biocalcification crises, and ‘ghost’ nanofossils represent a tool with which to test such claims.

Our imprint record shows that nanoplankton communities were more resilient to the environmental changes during the T-OAE – including high-CO₂ and warming (evident from independent proxies; 12 and references therein) – than the traditional nanofossil and CaCO₃ records suggest. However, several previously observed species-specific changes, such as declines in *Schizosphaerella punctulata* and nannoconids during the T-OAE and OAE1a, respectively, may still represent primary responses of nanoplankton to environmental change (Data S1 and S2). At the community-level, however, the imprint record shows that nanoplankton flourished during the T-OAE, and their resilience is supported by observations of increased speciation rates and an absence of elevated extinctions at the T-OAE and OAE1a (Data S1 to S3).

The abundance of prasinophyte algae in many T-OAE intervals is seen as a rise to dominance at the expense of nanoplankton (16), but the close association of imprints and prasinophyte fossils observed here demonstrates that both groups coexisted or occurred in close

succession (e.g. Fig. 1C). Near-monospecific assemblages of prasinophytes during the T-OAE likely represent persistent algal blooms (22), and similarly, the monospecific concentrations of nannofossil imprints (Fig. 2F, Figs. S3B and S7A) are pellets or aggregates that provide snapshots of high-dominance communities. Rather than being considered casualties of the T-OAE, our findings indicate nanoplankton continued to draw down CO₂ and sequester carbon in seafloor sediments, which in the long-term likely expedited the termination of the event. However, high production, blooms and potential toxicity (23), suggest that in the short-term, like prasinophytes, nanoplankton fueled anoxia through eutrophication and increased accumulation of organic matter at the seafloor, enhanced by coccolith ballasting (24) (Fig. 3).

Our records of ‘ghost’ nannofossils, discovered using unconventional methods, indicate no evidence for biocalcification crises during the studied Mesozoic OAEs, at least for plankton that form calcite, the more stable CaCO₃ polymorph compared to aragonite. Instead, these findings show how diagenesis can completely reshape the geological archive and highlight that a literal reading of the fossil record can mislead interpretations. Given that atmospheric CO₂ concentrations are currently rising at unprecedented rates, the use of individual OAEs as past analogues of current change may be premature, because carbon-input rates – and therefore the duration and intensity of surface water OA – remain uncertain for these events (10, 21). Nevertheless, our imprint record demonstrates the resilience of nanoplankton communities during multiple past global warming events, and equally, shows that plankton proliferation can accelerate the development of OAEs. Our findings also indicate that the conditions that prevailed during OAEs may become more prevalent (25, 26), with plankton blooms and hypoxic dead zones becoming widespread across globally warming oceans.

References and Notes

1. J. C. Orr *et al.*, Anthropogenic ocean acidification over the twenty-first century and its impact on calcifying organisms. *Nature* **437**, 681–686 (2005).
2. S. C. Doney, D. S. Busch, S. R. Cooley, K. J. Kroeker, The impacts of ocean acidification on marine ecosystems and reliant Human communities. *Annu. Rev. Environ. Resour.* **45**, 83–112 (2020).
3. B. Rost, U. Riebesell, “Coccolithophores and the biological pump: responses to environmental changes” in *Coccolithophores: molecular processes to global impact*, H. R. Thierstein, J. R. Young, Eds. (Springer, Berlin, 2004), pp. 99–125.
4. U. Riebesell, *et al.*, Reduced calcification of marine plankton in response to increased atmospheric CO₂. *Nature* **407**, 364–367 (2000).
5. M. D. Iglesias-Rodriguez *et al.*, Phytoplankton calcification in a high-CO₂ world. *Science* **320**, 336–340 (2008).
6. L. Schlüter *et al.*, Adaptation of a globally important coccolithophore to ocean warming and acidification. *Nat. Clim. Change* **4**, 1024–1030 (2014).
7. J. Meyer, U. Riebesell, Reviews and Syntheses: Responses of coccolithophores to ocean acidification: a meta-analysis. *Biogeosciences* **12**, 1671–1682 (2015).
8. L. T. Bach, U. Riebesell, M. A. Gutowska, L. Federwisch, K. G. Schulz, A unifying concept of coccolithophore sensitivity to changing carbonate chemistry embedded in an ecological framework. *Prog. Oceanogr.* **135**, 125–138 (2015).

9. S. J. Gibbs, S. A. Robinson, P. R. Bown, T. Dunkley Jones, J. Henderiks, Comment on “Calcareous Nannoplankton Response to Surface-Water Acidification Around Oceanic Anoxic Event 1a”. *Science* **332**, 175 (2011).
10. B. Hönisch *et al.*, The geological record of ocean acidification. *Science* **335**, 1058–1063
5 (2012).
11. J. Pálffy, P. L. Smith, Synchrony between Early Jurassic extinction, oceanic anoxic event, and the Karoo-Ferrar flood basalt volcanism. *Geology* **28**, 747–750 (2000).
12. H. C. Jenkyns, Geochemistry of oceanic anoxic events. *Geochem. Geophys. Geosyst.* **11**, Q03004 (2010).
- 10 13. C. Downie, Microplankton from the Kimeridge Clay. *Quart. J. Geol. Soc. Lond.* **112**, 413–434 (1956).
14. D. J. Batten, Coccolith moulds in sedimentary organic matter and their use in palynofacies analysis. *J. Micropaleont.* **4**, 111–116 (1985).
- 15 15. M.-C. Janin, The imprints of Cenozoic calcareous nannofossils from polymetallic concretions: Biostratigraphic significance for two crusts from the Central Pacific (Line Islands Ridge and Mid-Pacific Mountains). *Abh. Geol. B.-A.* **59**, 121–141 (1987).
16. R. B. Bucefalo Palliani, E. Mattioli, J. B. Riding, The response of marine phytoplankton and sedimentary organic matter to the early Toarcian (Lower Jurassic) oceanic anoxic event in northern England. *Mar. Micropaleontol.* **46**, 223–245 (2002).
- 20 17. D. B. Kemp, V. Baranyi, K. Izumi, R. D. Burgess, Organic matter variations and links to climate across the early Toarcian oceanic anoxic event (T-OAE) in Toyora area, southwest Japan. *Palaeogeogr. Palaeoclimatol. Palaeoecol.* **530**, 90–102 (2019).

18. C. D. Curtis, Diagenetic alteration in black shales. *J. Geol. Soc.* **137**, 189–194 (1980).
19. T. Müller *et al.*, Ocean acidification during the early Toarcian extinction event: Evidence from boron isotopes in brachiopods. *Geology* **48**, 1184–1188 (2020).
20. Q. Li *et al.*, Testing for ocean acidification during the Early Toarcian using $\delta^{44/40}\text{Ca}$ and $\delta^{88/86}\text{Sr}$. *Chem. Geol.* **574**, 120228 (2021).
21. B. D. A. Naafs *et al.*, Gradual and sustained carbon dioxide release during Aptian Oceanic Anoxic Event 1a. *Nat. Geosci.* **9**, 135–139 (2016).
22. S. M. Slater, R. J. Twitchett, S. Danise, V. Vajda, Substantial vegetation response to Early Jurassic global warming with impacts on oceanic anoxia. *Nat. Geosci.* **12**, 462–467 (2019).
23. A. Houdan *et al.*, Toxicity of coastal coccolithophores (Prymnesiophyceae, Haptophyta). *J. Plankton Res.* **26**, 875–883 (2004).
24. G. Fischer, G. Karakaş, Sinking rates and ballast composition of particles in the Atlantic Ocean: implications for the organic carbon fluxes to the deep ocean. *Biogeosciences* **6**, 85–102 (2009).
25. S. Rivero-Calle, A. Gnanadesikan, C. E. Del Castillo, W. M. Balch, S. D. Guikema, Multidecadal increase in North Atlantic coccolithophores and the potential role of rising CO_2 . *Science* **350**, 1533–1537 (2015).
26. R. J. Diaz, R. Rosenberg, Spreading dead zones and consequences for marine ecosystems. *Science* **321**, 926–929 (2008).

References and Notes in Supplementary Materials

27. S. Danise, R. J. Twitchett, C. T. S. Little, M.-E. Clémence, The impact of global warming and anoxia on marine benthic community dynamics: An example from the Toarcian (Early Jurassic). *PLoS ONE* **8**, e56255 (2013).
28. S. Danise, R. J. Twitchett, C. T. S. Little, Environmental controls on Jurassic marine ecosystems during global warming. *Geology* **43**, 263–266 (2015).
29. N. Hudson, “The Middle Jurassic of New Zealand: a study of the lithostratigraphy and biostratigraphy of the Ururoan, Temaikan and Lower Heterian Stages (?Pliensbachian to ?Kimmeridgian),” thesis, The University of Auckland, Auckland, New Zealand (1999).
30. N. Hudson, Stratigraphy and correlation of the Ururoan and Temaikan Stage (Lower–Middle Jurassic, ?Sinemurian–Callovia) sequences, New Zealand. *J. R. Soc. N. Z.* **33**, 109–147 (2003).
31. G. R. Stevens, Dactylioceratidae (Cephalopoda, Ammonoidea) from the Early Jurassic of New Zealand. *New Zealand J. Geol. Geophys.* **51**, 317–330 (2008).
32. G. R. Stevens, The ammonite genus *Harpoceras* (Early Jurassic) in New Zealand. *New Zealand J. Geol. Geophys.* **50**, 377–386 (2007).
33. K. R. Martin, Upper Triassic to Middle Jurassic stratigraphy of south-west Kawhia, New Zealand. *New Zealand J. Geol. Geophys.* **18**, 909–938 (1975).
34. F. Brotzen, De Geologiska resultaten från Borringarna vid Höllviken. Del I: Kritan. *Sver. Geol. Unders., Ser. C* **465**, 1–64 (1945).
35. F. Brotzen, De Geologiska resultaten från Borringarna vid Höllviken. Del II: Undre Kritan och Trias. *Sver. Geol. Unders., Ser. C* **505**, 1–48 (1950).

36. V. Vajda, Aalenian to Cenomanian terrestrial palynofloras of SW Scania, Sweden. *Acta Palaeontol. Pol.* **46**, 403–426 (2001).
37. P. Monaco, F. J. Rodríguez-Tovat, A. Uchman, Ichnological analysis of lateral environmental heterogeneity within the Bonarelli Level (uppermost Cenomanian) in the classical localities near Gubbio, Central Apennines, Italy. *Palaios* **27**, 48–54 (2012).
38. P. R. Bown, J. R. Young, “Techniques” in *Calcareous Nannofossil Biostratigraphy (British Micropalaeontological Society Publications Series)*, P. R. Bown, Ed. (Chapman and Kluwer Academic, London, 1998), pp. 16–28.
39. E. Erba, C. Bottini, G. Faucher, G. Gambacorta, S. Visentin, The response of calcareous nannoplankton to Oceanic Anoxic Events: The Italian pelagic record. *Boll. Soc. Paleontol. Ital.* **58**, 51–71 (2019).
40. D. B. Kemp, A. L. Coe, A. S. Cohen, L. Schwark, Astronomical pacing of methane release in the Early Jurassic period. *Nature* **437**, 396–399 (2005).
41. A. S. Cohen, A. L. Coe, S. M. Harding, L. Schwark, Osmium isotope evidence for the regulation of atmospheric CO₂ by continental weathering. *Geology* **32**, 157–160 (2004).
42. K. Littler, S. P. Hesselbo, H. C. Jenkyns, A carbon-isotope perturbation at the Pliensbachian–Toarcian boundary: evidence from the Lias Group, NE England. *Geol. Mag.* **147**, 181–192 (2010).
43. C. R. Scotese, *Atlas of Earth History, PALEOMAP Project* (Arlington, TX, 2001).
44. C. R. Scotese, “Map Folio 27, Early Cretaceous, (early Aptian, 121.8 Ma), PALEOMAP PaleoAtlas for ArcGIS, Cretaceous Paleogeographic, Paleoclimatic and Plate Tectonic Reconstructions, PALEOMAP Project,” vol. 2 (Evanston, IL, 2013).

45. C. R. Scotese, “Atlas of Late Cretaceous Maps, PALEOMAP Atlas for ArcGIS, The Cretaceous, Maps 16–22, Mollweide Projection, PALEOMAP Project,” vol. 2 (Evanston, IL, 2014).

5 **References and Notes in Data S1–S3**

46. E. Erba, Calcareous nannofossils and Mesozoic oceanic anoxic events. *Mar. Micropaleontol.* **52**, 85–106 (2004).

47. E. Mattioli, B. Pittet, Spatial and temporal distribution of calcareous nannofossils along a proximal–distal transect in the Lower Jurassic of the Umbria–Marche Basin (central Italy). *Palaeogeogr. Palaeoclimatol. Palaeoecol.* **205**, 295–316 (2004).

48. E. Mattioli *et al.*, Phytoplankton evidence for the timing and correlation of palaeoceanographical changes during the early Toarcian oceanic anoxic event (Early Jurassic). *J. Geol. Soc.* **161**, 685–693 (2004).

49. F. Tremolada, B. van de Schootbrugge, E. Erba, Early Jurassic schizosphaerellid crisis in Cantabria, Spain: Implications for calcification rates and phytoplankton evolution across the Toarcian oceanic anoxic event. *Paleoceanography* **20**, PA2011 (2005).

50. E. Mattioli, B. Pittet, G. Suan, S. Mailliot, Calcareous nannoplankton changes across the early Toarcian oceanic anoxic event in the western Tethys. *Paleoceanography* **23**, PA3208 (2008).

51. G. Suan, E. Mattioli, B. Pittet, S. Mailliot, C. Lécuyer, Evidence for major environmental perturbation prior to and during the Toarcian (Early Jurassic) oceanic anoxic event from the Lusitanian Basin, Portugal. *Paleoceanography* **23**, PA1202 (2008).

52. M. Hermoso, L. Le Callonnec, F. Minoletti, M. Renard, S. P. Hesselbo, Expression of the Early Toarcian negative carbon-isotope excursion in separated carbonate microfractions (Jurassic, Paris Basin). *Earth Planet. Sci. Lett.* **277**, 194–203 (2009).
53. E. Mattioli, B. Pittet, L. Petitpierre, S. Mailliot, Dramatic decrease of pelagic carbonate production by nanoplankton across the Early Toarcian anoxic event (T-OAE). *Glob. Planet. Change* **65**, 134–145 (2009).
54. A. Trecalli, J. Spangenberg, T. Adatte, K. B. Föllmi, M. Parente, Carbonate platform evidence of ocean acidification at the onset of the early Toarcian oceanic anoxic event. *Earth Planet. Sci. Lett.* **357–358**, 214–225 (2012).
- 10 55. Á. Fraguas, M. J. Comas-Rengifo, J. J. Gómez, A. Goy, The calcareous nannofossil crisis in Northern Spain (Asturias province) linked to the Early Toarcian warming-driven mass extinction. *Mar. Micropaleontol.* **94–95**, 58–71 (2012).
56. M. Hermoso *et al.*, Dynamics of a stepped carbon-isotope excursion: Ultra high-resolution study of Early Toarcian environmental change. *Earth Planet. Sci. Lett.* **319–320**, 45–54
15 (2012).
57. M.-E. Clémence, S. Gardin, A. Bartolini, New insights in the pattern and timing of the Early Jurassic calcareous nannofossil crisis. *Palaeogeogr. Palaeoclimatol. Palaeoecol.* **427**, 100–108 (2015).
58. C. E. Castello, E. Erba, Calcareous nannofossil biostratigraphy and paleoceanography of the
20 Toarcian Oceanic Anoxic Event at Colle Di Sogno (Southern Alps, Northern Italy). *Riv. Ital. Paleontol. Stratigr.* **121**, 297–327 (2015).

59. M. Hermoso, S. P. Hesselbo, Comment on “New insights in the pattern and timing of the Early Jurassic calcareous nannofossil crisis” by M. E. Clémence et al. [Palaeogeography Palaeoclimatology Palaeoecology 427 (2015) 100–108]. *Palaeogeogr. Palaeoclimatol. Palaeoecol.* **457**, 422–423 (2016).
- 5 60. S. Gardin, A. Bartolini, Reply to the comment on “New insights in the pattern and timing of the Early Jurassic calcareous nannofossil crisis” by M. Clémence, S. Gardin, S. A. Bartolini [Palaeogeography Palaeoclimatology Palaeoecology 427 (2015) 100–108]. *Palaeogeogr. Palaeoclimatol. Palaeoecol.* **457**, 424–427 (2016).
61. M. Reolid, J. Iwańczuk, E. Mattioli, I. Abad, Integration of gamma ray spectrometry, magnetic susceptibility and calcareous nannofossils for interpreting environmental perturbations: An example from the Jenkyns Event (lower Toarcian) from South Iberian Palaeomargin (Median Subbetic, SE Spain). *Palaeogeogr. Palaeoclimatol. Palaeoecol.* **560**, 110031 (2020).
- 10
62. A. Menini, E. Mattioli, S. P. Hesselbo, M. Ruhl, G. Suan, Primary versus carbonate production in the Toarcian, a case study from the Llanbedr borehole (Mochras Farm, Wales). *Geol. Soc. Spec. Publ.* **514** (2021).
- 15
63. Á. Fraguas, J. J. Gómez, A. Goy, M. J. Comas-Rengifo, The response of calcareous nannoplankton to the latest Pliensbachian–early Toarcian environmental changes in the Camino Section (Basque Cantabrian Basin, northern Spain). *Geol. Soc. Spec. Publ.* **514** (2021).
- 20
64. E. Erba, Nannofossils and superplumes: The early Aptian “nannoconid crisis”. *Paleoceanography* **9**, 483–501 (1994).

65. H. Weissert, A. Lini, K. B. Föllmi, O. Kuhn, Correlation of Early Cretaceous carbon isotope stratigraphy and platform drowning events: a possible link? *Palaeogeogr. Palaeoclimatol. Palaeoecol.* **137**, 189–203 (1998).
66. M. Cobianchi, V. Luciani, A. Menegatti, The Selli Level of the Gargano Promontory, Apulia, southern Italy: foraminiferal and calcareous nannofossil data. *Cretaceous Research* **20**, 255–269 (1999).
67. E. Erba, F. Tremolada, Nannofossil carbonate fluxes during the Early Cretaceous: Phytoplankton response to nutrification episodes, atmospheric CO₂, and anoxia. *Paleoceanography* **19**, PA1008 (2004).
68. H. Weissert, E. Erba, Volcanism, CO₂ and palaeoclimate: a Late Jurassic–Early Cretaceous carbon and oxygen isotope record. *J. Geol. Soc.* **161**, 695–702 (2004).
69. S. Méhay *et al.*, A volcanic CO₂ pulse triggered the Cretaceous Oceanic Anoxic Event 1a and a biocalcification crisis. *Geology* **37**, 819–822 (2009).
70. E. Erba, C. Bottini, H. J. Weissert, C. E. Keller, Calcareous nannoplankton response to surface-water acidification around Oceanic Anoxic Event 1a. *Science* **329**, 428–432 (2010).
71. T. J. Bralower, Calcareous nannofossil biostratigraphy and assemblages of the Cenomanian–Turonian boundary interval: Implications for the origin and timing of oceanic anoxia. *Paleoceanography* **3**, 275–316 (1988).
72. V. Luciani, M. Cobianchi, The Bonarelli Level and other black shales in the Cenomanian–Turonian of the northeastern Dolomites (Italy): calcareous nannofossil and foraminiferal data. *Cretaceous Research* **20**, 135–167 (1999).

73. P. Hardas, J. Mutterlose, Calcareous nannofossil assemblages of Oceanic Anoxic Event 2 in the equatorial Atlantic: Evidence of an eutrophication event. *Mar. Micropaleontol.* **66**, 52–69 (2007).

74. G. Faucher, E. Erba, C. Bottini, G. Gambacorta, Calcareous nannoplankton response to the latest Cenomanian Oceanic Anoxic Event 2 perturbation. *Riv. Ital. Paleontol. Stratigr.* **123**, 159–176 (2017).

Acknowledgments: We thank W. Foster, D. Murphy, M.-E. Clemence, H. Campbell, I. Raine, S. Monechi, K. Tanabe and Y. Takeda for their help with fieldwork.

Funding:

Wenner-Gren Foundation grant UPD2018-0114 (SMS, VV)

Swedish Research Council grants VR 2019-04524 (SMS), VR 2015-04264 (VV) and VR 2019-4061 (VV)

Carl Tryggers Foundation grant 19:380 (VV)

Natural Environment Research Council grant NE/I005641/1 (RJT)

Lund University Carbon Cycle Centre (VV)

Bolin Centre for Climate Research (SMS)

The Great Britain Sasakawa Foundation 4390 (SD)

Author contributions:

Conceptualization: SMS, PB, RJT, SD, VV

Methodology: SMS, PB, RJT, SD, VV

Investigation: SMS, PB, RJT, SD, VV

Visualization: SMS

Funding acquisition: SMS, RJT, VV, SD

Project administration: SMS

5 Supervision: PB, RJT, VV

Writing – original draft: SMS

Writing – review & editing: SMS, PB, RJT, SD, VV

Competing interests: Authors declare that they have no competing interests.

10 **Data and materials availability:** This report is based on material housed and curated by the
Department of Palaeobiology, Swedish Museum of Natural History, Stockholm, the
Department of Earth Sciences, The Natural History, London, and the Department of Earth
Sciences, University College London (see Data S5 for details). All data are available in the
main text or the supplementary materials.

15 **Supplementary Materials**

Materials and Methods

Figs. S1 to S15

References (27–74)

Data S1 to S5

20

Figure Captions

Fig. 1. ‘Ghost’ nanofossils imprinted on organic matter. (A) *Stauroolithites* sp. imprint on *Classopollis* spp. (pollen) [NHMUK PM FM 2355 (2)]. (B) *Crepidolithus impontus* imprints on *Cerebropollenites macroverrucosus* (pollen) [NHMUK PM FM 2355 (2)]. (C) *Bussonius prinsii* imprint on prasinophyte algae [NHMUK PM FM 2355 (2)]. (D–K) Imprints on amorphous organic matter. (D) *Bussonius prinsii* [NHMUK PM FM 2355 (2)]. (E) *Axopodorhabdus atavus* [NHMUK PM FM 2377 (1)]. (F) *Calyculus serrai* coccosphere [NHMUK PM FM 2377 (1)]. (G) *Axopodorhabdus* sp. [S043981]. (H) *Lotharingius hauffii* [S043957]. (I) *Calyculus* sp., *Stauroolithites* sp. and others [S043993]. (J) *Manivitella pemmatoidea* [S043946]. (K) *Stoverius achylosus* [S043941]. Blue images are inverted ‘virtual casts’. Scale bars in overviews of (A–C) are 10 μm , all other scale bars are 2 μm .

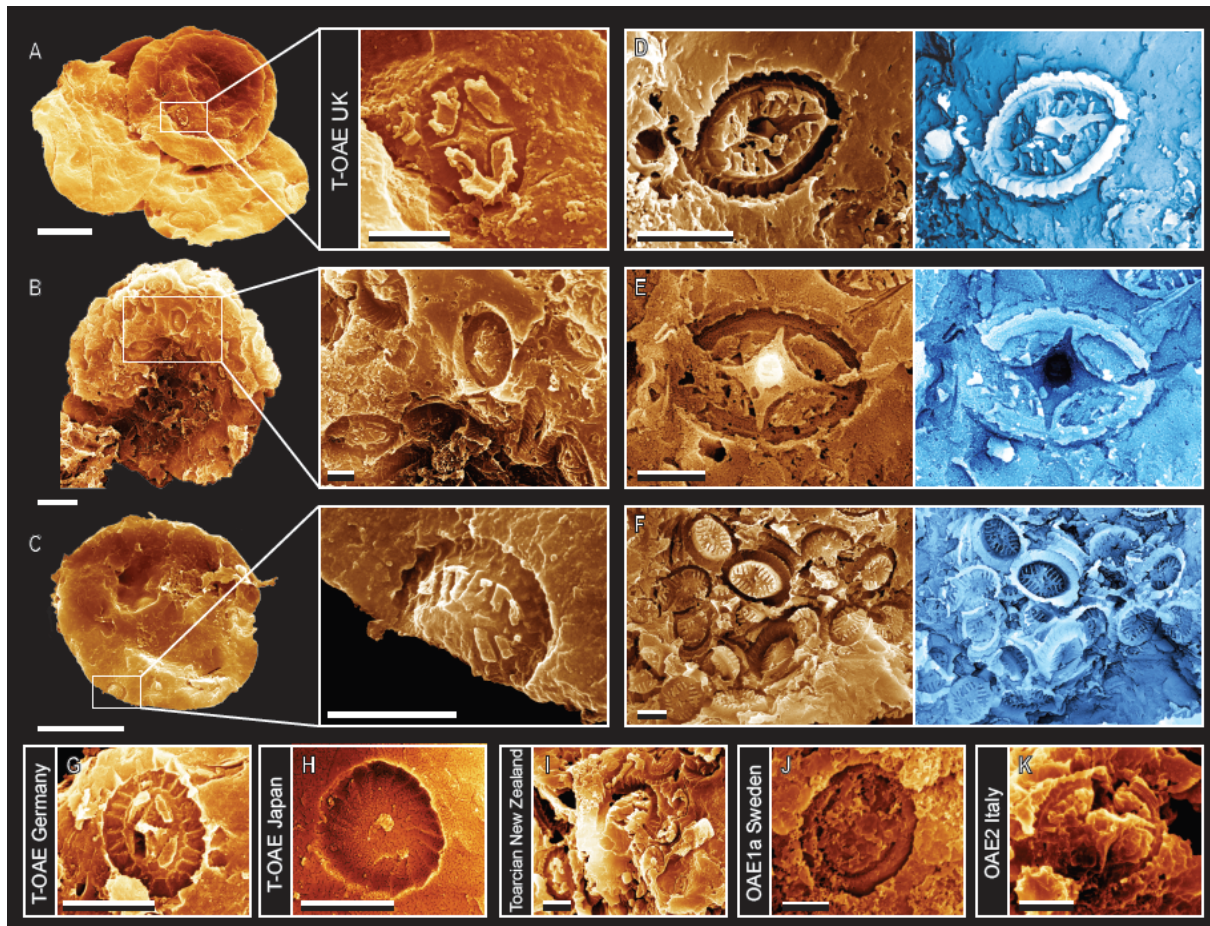


Fig. 2. ‘Ghost’ nannofossil, ‘body’ nannofossil and organic matter records through the T-OAE (Japan, UK), OAE1a (Sweden) and OAE2 (Italy). Imprints/area represents the number of imprints recorded across a standard area of organic matter. ‘Body’ fossil abundance categories: Abundant = >10% of particles; Common = >1–10%; Frequent = 0.1–1%; Rare = <0.1%; Very Rare = <20 specimens in total; Barren = no ‘body’ fossils. See Materials and Methods for further details, including richness and organic matter data collection methods. Note the different vertical scale for OAE2. See Fig. S14 for extended version that includes data from Germany and New Zealand. For raw data, see Data S4.

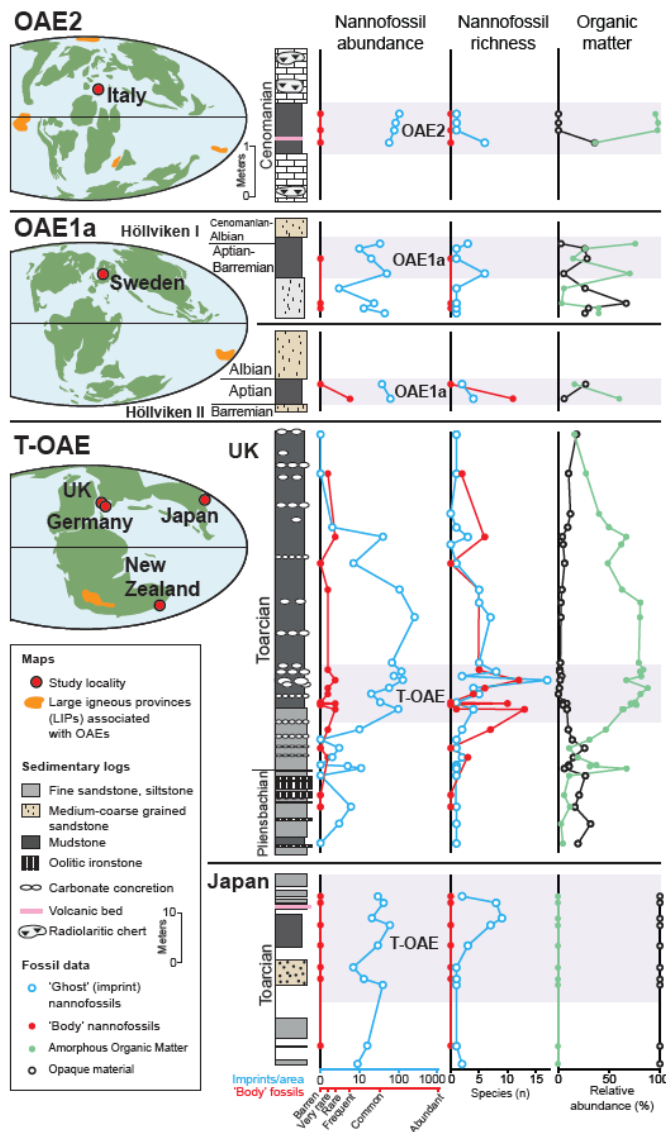


Fig. 3. Schematic summary of the major changes in phytoplankton groups through the T-OAE, showing changes in phytoplankton export and the formation of nannofossil imprints.

5 OMZ = Oxygen minimum zone. Note the expansion of the oxygen minimum zone during the OAE, and the acidic pore waters within sub-surface sediments post-OAE leading to the dissolution of nannoplankton 'body' fossils and the formation of imprints.

